Engineering on-demand Magnetic Core-shell Composite Wound Dressing Matrices via Electrohydrodynamic Micro Scale **Printing**

Baolin Wang[1,2], Xing Chen[1,2]* Zeeshan Ahmad[3], Jie Huang[4], Ming-Wei Chang[1,2,5]*

[1] Key Laboratory for Biomedical Engineering of Education Ministry of China, Zhejiang University, Hangzhou, 310027, P.R. China.

[2] Zhejiang Provincial Key Laboratory of Cardio-Cerebral Vascular Detection Technology and Medical Effectiveness Appraisal, Zhejiang University, Hangzhou, 310027, P.R. China.

[3] Leicester School of Pharmacy, De Montfort University, The Gateway, Leicester, LE1 9BH, UK.

[4] Department of Mechanical Engineering, University College London, London WC1E7JE, UK.

[5] Nanotechnology and Integrated Bioengineering Centre, University of Ulster, Jordanstown Campus, Newtownabbey, BT37 0QB, Northern Ireland, UK

*Email: mwchang@zju.edu.cn; Tel: +86(0)571-87951517

Keywords: coaxial; printing; matrices; drug release; wound dressings.

Abstract

In this study, electrohydrodynamic (EHD) printing was utilized to produce well-ordered, dual-drug loaded-magnetic core-shell matrices with high resolution. Coaxial EHD printing was used to load anesthetic lidocaine hydrochloride (LH) and antibiotic tetracycline hydrochloride (TH) in polycaprolactone (PCL) shell formulation and poly (ethylene oxide) (PEO) core formulation, respectively. It was found that when the concentration of PEO was 5% w/w, the fibers exhibited optimum morphology, which was applied in the fabrication of two drugs loaded core-shell fibers. In addition, adding iron oxide (Fe_3O_4) NPs and varying the concentration of TH within the PCL shell layer influenced mechanical properties, release behaviors and cell behaviors of coaxial EHD printing matrices. The addition of Fe_3O_4 NPs and increasing TH amount in the fibers would enhance the mechanical properties of the matrices. Results showed rapid release of LH located in the PEO core fibers while TH loaded in the shell PCL fibers was released sustainably from the coaxial printing matrices. In addition, the sustainable release period for PCL shell layer could be adjusted using Fe_3O_4 NPs under auxiliary magnetic field. The coaxial drug-loaded matrices also had good bioactivity, indicating the potential of the printed fibers in wound dressings.

1. Introduction

As the largest organ, the skin is very important in human body. It maintains homeostasis and prevents the invasion of microorganisms.[1] Some patients suffering from burns, trauma or other skin diseases may experience acute soreness and severe infections.[2] Thus, it is necessary to develop wound dressings which can provide both analgesic and healing effects for wound treatment; delivering dual therapeutic effects with controllable release kinetics.[3, 4] The wound dressing should have good biocompatibility, reduce pain and infection,[5] have the ability to absorb redundant exudates and keep a moist healing environment around the wound surface.[6, 7] Though some commercial products try to meet one or more of these needs, there is no simple approach to solve the above problems.[8, 9]Based on the mentioned ideas, it is necessary to develop a dual drug dosage form for wound dressing. Fibers with micron and nano scale are excellent candidates for this application as they are able to absorb wound exudate more efficiently, preventing the wound from drying up and protecting from bacterial infection whilst allowing gas permeation.[10, 11]

There are array of methods to fabricate fibrous wound dressings.[12-14] Among the different fibers preparation techniques, electrohydrodynamic (EHD) printing is very attractive for its simplicity and flexibility, which has been widely applied in many fields like stretchable electronics.[15, 16] EHD printing can digitally control the deposition of materials to produce well-ordered structures[17]. As wound dressings, the well-ordered fibers structures could be attached to the wound evenly, resulting in the drugs being applied to the wound homogenously. Several three-dimensional (3D) printing techniques have been used to produce aligned fibers. However, there are some limitations for current 3D printing methods and therefore need to be improved. For example, the stereolithography printing technology could only use photosensitive polymers or composites containing photopolymers[18].

Fused deposition modelling (FDM) involves heating the polymer in the extrusion nozzle until it melts for jetting. The appropriate materials for FDM remains limited since they must satisfy the ability to be pre-processed into polymer filaments[18]. However, EHD printing paves a way to fabricate micro to nano scale aligned fibers and overcome the limitations of these techniques. A range of materials can be applied in EHD printing as this process does not employ harsh processing conditions that could destroy the properties of materials incorporated in the printing solution for functional applications e.g. high temperature. Moreover, core-shell fibers used in drug delivery have great advantages. According to previous studies, different drugs were usually encapsulated into single fibers and core-shell fibers were fabricated via coaxial electrospinning [19, 20].Thus, the coaxial EHD printing technique were applied to encapsulate two functional drugs separately by PCL and PEO components.

A great number of synthetic and natural polymer composites have been widely applied in wound dressings in recent years. For example, polycaprolactone (PCL) and poly (ethylene oxide) (PEO) are conventional synthetic polymers which have been used for wound dressing.[21, 22] PCL is a synthetic, biodegradable and bioresorbable FDA approved polymer which belongs to the aliphatic polyesters family [23]. It is a semi-crystalline, hydrophobic polymer and its crystallinity tends to decrease as its molecular weight increases. Due to its high crystallinity and high hydrophobicity, its degradation can be delayed for an extended period of time.[24]. According to previous studies, the Fe_3O_4 NPs incorporated in polymer-based drug carriers respond to the external magnetic field. It has been reported that when there was no magnetic field, the magnetic moments of Fe_3O_4 NPs in the matrices were randomly oriented. While applying the external magnetic field, the magnetic moments of the particles tend to align with the magnetic fields and produce a bulk magnetic moment. The external magnetic field could stimulate the motion of Fe_3O_4 NPs and thus enhance the relaxation ability of the

polymeric chains, which subsequently expanded the whole structures, causing the enhancement of drug release [25, 26]. So Fe_3O_4 NPs could be incorporated in the PCL based fibers to improve the drug release rate. PEO is also a biocompatible polymer and one of the few synthetic polymers approved for internal use in personal care products and pharmaceuticals.[27] It is hydrophilic, and can be combined with PCL to form a complex dosage form and deliver various drugs to achieve both rapid and sustained drug release.

The drugs incorporated in our matrixes were lidocaine hydrochloride (LH) and tetracycline hydrochloride (TH). Lidocaine is a commonly used anesthetic in wound related pain management. Its incidence of allergic reactions was lower than the ester-type anesthetics such as procaine and tetracaine.[28] It also has some antibacterial action against *Escherichia coli* and *Staphylococcus aureus*.[28, 29] TH, which belongs to a group of broad-spectrum antibiotics and is normally applied to treat and control bacterial skin infections, was used as the model active compound.[30] In this work, coaxial nozzle-assisted EHD printing was used to encapsulate two different drugs within well–ordered fiber matrices for wound dressings. LH and TH were added to PEO and PCL separately by coaxial EHD printing to achieve the proposed dual release. LH encapsulated in the inner PEO layer would be released rapidly to relieve pain of the wound, while TH located in the outer PCL layer would be released sustainably to achieve the effect of promoting wound closure. Thus, this kind of aligned core-shell matrices had great potential to be applied in wound dressing. The coaxial structures of the fibers were observed using optical microscopy and scanning electron microscopy (SEM). The physical properties of the core-shell matrices were investigated by Fourier Transform infrared spectroscopy (FTIR), contact angle analysis, X-ray diffraction and tensile testing. The drug release profiles of LH and TH were detected separately.

2. Results and discussion

2.1. Fabrication of core-shell printed matrices

Figure 1a is the schematic diagram of the coaxial EHD printing system utilized in this study. The detailed inner structure of the coaxial nozzle is shown in Figure 1b. While Figure 1(b1-b4) show the cone-jet changing with increasing applied voltage during coaxial EHD printing process. To differentiate between the PCL and PEO solutions, the latter was dyed with Rhodamine B. When the high voltage was not applied to the coaxial nozzle and the flow rate of inner liquid and outer solution was set at 0.1 mL/h and 0.25 mL/h, respectively, there was a droplet containing both PCL solution and PEO solution hanging at the tip of the needle (Figure 1b1). Increasing the electric potential to around 1.5 kV resulted in dripping mode. During dripping mode (Figure 1b2), the pendant drops pinch off from the nozzle tip due to the gravitational force. Increasing electric force against the surface tension made the droplets fall more rapidly. Pulsating mode (Figure 1b3) appeared when the applied voltage reached to about 2.0 kV, and this mode have both the hemispherical shape and Taylor cone shape due to the unbalance of surface tension and the electric charge. Finally, the applied voltage was fixed at 2.6 kV, cone-jet mode was shown in Figure 1b4. This was the ideal parameters and movement speed of X-Y-Z stage was set at 80 mm/s at this model condition during coaxial EHD printing,[31] as shown in Figure 1b4. There are two different solutions observed during all modes, confirming the coaxial structure of the printing matrices.

2.2. Influence of the PEO concentration on coaxial structures

The concentration of PEO solutions found to have a significant effect on the structures and morphology of the coaxial fibers. According to previous references,[32, 33] the concentration of PCL solution applied in EHD printing are usually within the range 20 % - 25% w/w, and because PCL

solutions were used as the shell formulation, the concentration of PCL in coaxial EHD printing was fixed at 24% w/w, consistent with former experiments. The optimal polymer concentration varies with the type of polymer, its molecular weight, and manufacture technology. Moreover, the solvent type also has a significant effect. Though PEO solutions have been previously used in EHD printing process,[34] its application as the core solution in coaxial EHD printing process has not been reported before. Thus, in this paper, a series of PEO solutions were investigated during coaxial EHD printing process. To figure out two different solutions, PEO solution were dyed by Rhodamine B. **Figure 2**a shows the optical microscopy images of the resulting coaxial structures fabricated when using 5% w/w PEO (in glacial acetic acid) solutions. The flow rates of PEO solution and PCL solution were set at 0.1 mL/h and 0.25 mL/h, respectively. While the applied voltage was fixed at 2.6 kV. It could be found that coaxial EHD printing technology successfully fabricated coaxial filaments. All the filaments and the core PEO fibers were continuous, indicating the suitable range. When the concentration of PEO solutions increased from 2% w/w to 6% w/w, the diameter of the core in the coaxial filaments were significantly improved (Figure 2b). The whole diameter of the coaxial filaments did not show any remarkable difference (Figure 2c). The optical images (Figure 2a) is larger than fiber diameters shown in the figure 2c. This is due to the fact that the first printing layer normally presents flat morphology rather than cylindrical shape as a result of bigger contact area with the collecting substrate. However, the core-shell fibers prepared at the concentration of PEO solutions (6% w/w) present little smaller diameter compared that obtained from the concentration of PEO solutions (5% w/w). It should be noted that the core-shell fibers prepared at the concentration of PEO solutions with 6% w/w were not uniform and the edges of the fibers were not smooth (as shown in supporting information). The core/shell ratio changing with improving PEO concentrations were measured and data were plotted as shown in Figure 2d. Due to the little change in shell diameter and

increasing core diameter, the core-shell ratio increased with improving PEO concentrations. Therefore, to maximize the PEO composition and achieve therapeutic effect, PEO solutions with 5% w/w concentration were selected for subsequent experiments.

Figure 3 presents the SEM images with different magnifications of core-shell printed matrices loaded without Fe_3O_4 NPs and with 1.1% w/w TH in PCL layer. It is found that the matrices showed well-ordered structures (Figure 3a), and the core-shell fibers were stacked precisely (Figure 3b). The width between two adjacent fibers were 500 μm. Figure 3c is the SEM image of cross section of these kinds of coaxial filaments. Due to the elasticity of the fibers, the fibers showed adhesion morphology. After immersing the core-shell structures in DI water to remove core PEO fibers, hollow structures could be observed (Figure 3d), indicating the success of coaxial filaments produced by this method.

Figure 4 show inclined SEM images of core-shell printed matrices of magnetic core-shell printed matrices loaded with different concentrations of TH. The structures of all patterned matrices are observed. Figure 4a-d are SEM images of the core-shell printed matrices with Fe_3O_4 NPs where the concentration of TH was increased from 0.55% w/w to 2.2% w/w. The results showed that increasing the concentration of TH reduces of filaments diameter and making the printing process unstable, and there were some voids found insides the matrices with 2.2% w/w TH (Figure 4d and 4d1). Also, the amount of Fe_3O_4 NPs in the printing solutions was small and had no significant influence on the core-shell fiber formation. On the other hand, as there was more TH incorporated in the PCL shell, the residual solvent could evaporate more rapidly under the application of an electric field and the fusion between adjacent fibers only happened in matrices with lower TH concentrations (Figure 4a1-c1). Furthermore, increasing the concentration of TH helped produce fibers with larger diameters and smooth surfaces (Figure 4a2-4d2). Compared with the non-magnetic matrices and the addition of

Fe_3O_4 NPs in the matrices showed no significant difference with respect to morphology and structure of matrices, which is in accordance with previous study.[23]

2.3. Hydrophilicity and Fourier transform infrared spectroscopy of core-shell matrices

The surface wettability of wound dressings has a significant effect on drug release behaviors and comfort of the wound,[35] The surface wettability of five different kinds of matrices was investigated through detecting direct contact angles (CAs) between a phosphate buffer solution (PBS) droplet (1 µL, pH 7.4) and the surface of the matrices, as shown in **Figure 5**a. Figure 5b presents the detail values of five matrices samples with varying TH concentrations and Fe_3O_4 NPs. Referred to previous research, pure PCL fibers are high hydrophobic, while pure PEO fibers are hydrophilic.[36, 37] The initial contact angle for the magnetic core-shell matrices loaded with 0.55% TH was 93.7 ± 5.1°, showing insignificant difference after 5 mins to 93.0 ± 6.2° (Figure 5ii and 5b). While increasing the amount of TH in the magnetic core-shell matrices could improve the hydrophobicity of the matrices, and the initial contact angle would be increased with higher difference after 5 minutes' period. The initial contact angle for magnetic matrices loaded with 1.65% TH was 106.6 ± 4.44°, and the contact angle of this matrix was just 100 ± 4.4° after 5 min (Figure 5iv and 5b). However, for the magnetic core-shell matrices loaded with 2.2% TH, the increased concentration of TH reduced the initial contact angle significantly to 80.0 ± 9.62° and to 63.8 ± 2.6° after 5 min (Figure 5v and 5b). This is mainly due to the non-uniform morphology of this kind of matrix (Figure 4d and 4d1). In addition to this, incorporating Fe_3O_4 NPs into the core-shell matrices made the structures more hydrophilic, as the initial contact angle for non-magnetic matrices loaded with 1.1% TH was 105 ± 3.1° that was higher than magnetic matrices loaded with TH with same concentration (Figure 5i and 5b). These results mimic those seen in previous studies.[38] It means that inner PEO material had no effect on the

hydrophobicity of the matrices and indicates PEO was entirely encapsulated within the PCL fibers.

Fourier transform infrared spectroscopy (FTIR) was applied to confirm the chemical composition of the matrices within the range 4000-500 cm^{-1}. Figure 5c and 5d show the FTIR spectrum of pure materials and core-shell printed matrices, respectively. Here, characteristic absorption bands for PEO could be observed in Figure 5c, band at 1967 cm^{-1} belongs to asymmetric stretching, the band at 1473 cm^{-1} is assigned to CH$_2$ scissoring, C-O-C stretching resulted in band at 1101 cm^{-1}, CH$_2$ twisting mode was at 961 cm^{-1} and CH$_2$ wagging mode was at 840 cm^{-1},[34, 39] PCL polymer generates a strong carbonyl (C=O) peak at 1729 cm^{-1} and other absorptions between 2868 and 2949 cm^{-1} which caused by methylene (CH$_2$) groups.[23] Similar bands were found in spectrums for all five kinds of matrices as shown in Figure 5d. Figure 5c also shows that characteristic absorption peaks for TE-HCL mainly appeared at 1246 cm^{-1}(C-N), 1288 cm^{-1}(C-H stretching vibration) and 1460 cm^{-1} (O-H stretching vibration) for all matrices containing this drug.[34] Besides, it is necessary to note that the absorption peak at 780 cm^{-1}, related to the aromatic C-H, confirms the existence of LH in all matrices samples.[40] A characteristic band of Fe$_3$O$_4$ NPs at 580 cm^{-1}, which is attributed to the Fe-O band, were not found in the core-shell printed matrices[41]. This phenomenon happened for the reason the amount of Fe$_3$O$_4$ NPs in solutions is limited, and there is a possibility that the peaks of Fe$_3$O$_4$ NPs were covered by peaks of other materials. FTIR results made it clear that the materials components remain stable during coaxial EHD printing process.

2.4. Mechanical properties and XRD analysis

There have been several studies showing how the addition of metallic nanoparticles in the polymer fibers can enhance the mechanical properties of the resulting matrices.[42, 43] In this work, the

addition of both TH and Fe_3O_4 NPs have an effect on mechanical properties of core-shell printed matrices. **Figure 6**a-c show the shape change of core-shell printed matrices loaded with Fe_3O_4 NPs and 1.1% w/w TH during the tensile test process. It can be observed that the drawing force applied stretched the matrices until they fractured. Figure 6d shows the mechanical properties of five kinds of coaxial EHD printing matrices, and Figure 6e is the result of elastic modulus of the matrices. Matrices with 0.55% w/w TH and Fe_3O_4 NPs had rather low tensile strain (~349%) and lowest tensile strength (~1.7 MPa). The tensile strain and tensile strength of magnetic matrices with 1.1% w/w TH were 275% and 4.3 MPa, separately. As for the matrices loaded Fe_3O_4 NPs and 1.65% w/w TH, the tensile strain and strength were 364% and 6.3 MPa, respectively. Magnetic matrices with 2.2% w/w had highest tensile strain and tensile strength, which were 601% and 7.7 MPa, separately. However, for the non-magnetic matrices with 1.1% w/w, the tensile strain was 337% and the tensile strength was 3.3 MPa. The results showed that increasing the amount of TH in the PCL polymer and adding Fe_3O_4 NPs in the filaments could improve the mechanical properties of the matrices. As shown in Figure 6d, the elastic modulus which was calculated by the values of tensile strain and tensile strength, could be enhanced by improving the concentration of TH and adding some Fe_3O_4 NPs in the filaments. It might because increasing TH quantity caused the larger fiber diameter (Figure 4), leading this kind of matrices take more strength and could be stretched longer.

XRD analysis was conducted to detect any changes in the physical form of the drugs and polymers before and after core-shell printed matrices. As shown in Figure 6f and 6g, for pure PCL, the sharp diffraction peaks at $2\theta = 23.5°$ and $2\theta = 21.3°$ indicated PCL crystalline nature.[44] These peaks were both observed but weakened in five kinds of matrices after coaxial printing, which suggested the decrease of PCL crystallinity. The neat PEO shows two sharp feature peaks around $2\theta = 19.1°$ and $2\theta = 23.2°$.[45] There was only first PEO peaks related to PEO crystals also appeared in all five kinds of

matrices, however, this peak around $2\theta = 19.1°$ was weaker than for neat PEO material, indicating the existence of same PEO crystalline structure in the coaxial EHD printing structures, with a crystallinity degree lower than in the raw material. In addition, the crystallinity peaks observed in the XRD pattern form pure TH and LH disappeared in five complex matrices, and this suggested that TH and LH were amorphous in the core-shell printed matrices. These amorphous drugs in the complex matrices are advantageous for a drug delivery system because it improves drug release and bioavailability.[46] The amorphous drug showed a higher dissolution rate and led to a higher bioavailability for poorly soluble drugs. Meanwhile, the amorphous phase presented higher free energy, which could increase the exposure of hydrophobic and hydrophilic functional groups improving the wettability[47]. As for the crystalline peaks of Fe_3O_4 NPs disappearing in the XRD pattern of magnetic matrices, it might be the reason amount of Fe_3O_4 NPs was limited.

2.5. *In-vitro* drug release

Figure 7 displays cumulative drug release profiles from the printed matrices. The release kinetics of TH from four magnetic matrices was also investigated in vitro for 192 h (Figure 7a). Biphasic release profiles were observed for all samples; beginning with a rapid initial release stage (up to 0.5 h) followed by a slow release phase (from 0.5 h to 192 h). 45.9%, 62.3%, 79.0% and 78.6% of TH was released rapidly from matrices with 0.55%, 1.1%, 1.65% and 2.2% w/w TH carriers within the first hour of release studies, respectively. The quantity of TH release approaches 68.4%, 90.7%, 93.7%, and 92.4% after 192 h for matrices with 0.55%, 1.1%, 1.65% and 2.2% w/w TH, respectively. The rapid burst release is due to the reason that drug molecule distribution near the filament surface, which were caused by the drying process.[48] The results presented here show that the drug released from matrices with higher drug concentration had a faster release rate, which was in accordance with

previous studies.[49] To quantify the TH drug release mechanisms, a zero-order, first order, Higuchi and Korsmeyer-Peppas models were applied to fit the obtained release data. As shown in Table 1, the Korsmeyer-Peppas model had the highest correlation coefficient, and the n values were 0.0719, 0.0346, 0.0444, and 0.0389 for core-shell printed matrices with 0.55%, 1.1%, 1.65%, and 2.2% w/w TH, respectively. These values are lower than 0.45, suggesting the primary Fickian diffusion release mechanism of the TH in all the coaxial printing samples.

Drug release from magnetic matrices with 1.1% w/w TH and non-magnetic matrices with same drug concentration with the aid of an external AMF trigger was assessed over a 10 h time frame, and the release profile of the magnetic matrices with 1.1% w/w TH in the normal environment is also displayed (Figure 7b). It can be observed that the non-magnetic matrices had the slowest release rate compared to the other magnetic samples even though with the aid of AMF. For the magnetic samples, the introduction of AMF (40 kHz) around core-shell printed matrices vials induced greater drug release after 1 h compared to non-treated samples. The non-magnetic matrices released only 48.0% after 1 h under AMF environment, while the cumulative release of TH in the magnetic sample was 59.7%, which was much higher than the non-magnetic samples. After 600 min period of release, the cumulative release of TH in non-magnetic sample and magnetic sample were 65.9% and 72.9%, respectively. This can be explained by the reason that in the AMF environment, the motivated activity of Fe_3O_4 NPs could cause intensified motion of molecules within the polymeric filaments. Fe_3O_4 NPs also have the potential to produce heat influenced by AMF.[50] Because of same concentration for LH in all samples, only magnetic matrices was applied to study LH release with and without the aid of external AMF (Figure 7c). At the initial 5 min, the cumulative release of LH in same sample with and without AMF were 60.4% and 65.8%, respectively. While the cumulative release of LH in samples with and without AMF were 68.3% and 90.1%, respectively. Due to the reason that LH was contained

in PEO, which can be dissolved in PBS, the release rate of LH was more rapid than the release speed of TH. In addition to this, the induction of AMF could improve the release rate of LH. Thus, for core-shell printed matrices as wound dressings, LH could be released at a very fast speed and achieve the effect of anesthesia, while the sustained release of TH can heal the wound.

2.6. *In-vitro* biological test

The antimicrobial activity of the printed matrices was investigated using *S. aureus* (Gram +) as the test microorganism. All five kinds of core-shell printed matrices were applied for assessment. **Figure 8**a shows the disc samples to form inhibition zones after 24 h incubation. The incubation zones were evident with all matrices samples. Figure 8b shows the graph of inhibition zone area of the five samples and control group. There was no inhibition area found for control group. With respect to the core-shell printed matrices, as TH concentration increased, the inhibition zone area significantly increased. The inhibition zone areas for non-magnetic matrices and magnetic matrices loaded with same concentration of TH were almost identical, indicating that the Fe_3O_4 NPs had no effect against the bacteria. The antibacterial properties of the core-shell printed matrices were also measured against *S. aureus* (Gram +). The difference in antibacterial proliferation among different matrices is shown in Figure 8c. If there is a high concentration of bacteria contained in the vessel, the liquid/sample is very turbid.[51] The absorbance value of the broth was detected to indicate the amount of bacteria contained in this broth. As shown in Figure 8c, *S. aureus* treated with the matrices showed a decrease of number of bacteria compared to the control group. It was observed that increasing the concentration of TH in the matrices would increase the activity against *S. aureus* significantly. The relative viability of *S. aureus* incubated with magnetic matrices loaded with 2.2% TH was only 42%. Moreover, the addition of Fe_3O_4 NPs showed no obvious influence on anti-bacteria activity.

In this study, the potential toxic effects of core-shell printed matrices due to solvent processing and additional components including TH, LH and Fe_3O_4 NPs were investigated. Morphologies of cells cultured on five different kinds of matrices and culture dish without samples were assessed using fluorescent microscopy after 3 days culture (Figure 9a-f). It can be observed that the number of cells on the matrices loaded with Fe_3O_4 NPs were evidently higher than that of matrices without Fe_3O_4 NPs. Besides, there were most cell on the matrices loaded with 1.1% w/w TH, indicating that moderate TH concentration could improve cell proliferation on matrices. Compared with cells culture just on culture dish, cell on the matrices had more extension and shape of cells were longer, this could be observed in the insets of **Figure 9**a-e. Cell viability reflects the potential toxic risks of printing matrices *in vitro*, presented as a percentage of viable cells within the total cell population.[52] The CCK-8 test was applied to evaluate the cytotoxicity of these matrices after 3 days culture. As shown in **Figure 10**a, cell viability for core-shell printed matrices loaded with 0.55%, 1.1%, 1.65%, and 2.2% w/w TH were 71.1%, 97.0%, 105.3%, 97.9% and 68.9% compared to control (100%), indicating that the addition of Fe_3O_4 NPs and TH concentration had significant influence on cell viability. The results showed that by incorporating Fe_3O_4 NPs could enhance cell viability. Moreover, cell viability could be increased by improving the concentration of TH from 0.55% to 1.1% w/w and be decreased by continuing the increase of TH concentration to 2.2%, which are in accordance with the fluorescent images. These results indicated that excellent biocompatibility of core-shell printed matrices, which can be applied in wound dressings.

In vitro wound healing scratch assay was conducted to investigate the effect of core-shell printed matrices on cell migration. **Figure 11** illustrated the gap closure of the scratched monolayer of L929 cells in the presence of both control and different core-shell printed matrices, at initial time and after

24 h, and 72 h of incubation. In order to evaluate the kinetic of the wound healing, the percentage of gap closure was determined using the ImageJ software. The curves of the percentage of gap closure as a function of time are presented in Figure 10b. It was found that, after the initial 24 h of incubation, the monolayer appeared irregular with cellular retractions (Figure 11(a1-f1)). Cell polarization with protrusions and proliferation were locally seen in the boundary cells for all samples. The highest migration rate (about 16%) was observed for magnetic samples loaded with 2.2% TH. Besides, at the first 24 h, the migration rate increased with increasing loading concentration of TH. After incubation of 72h, migratory cells from the border zone to the denuded area was evidently observed (Figure 11a2-f2) and the cell densities in the border zone turned to decrease. Moreover, the cells migration was almost covered whole scratch area for the magnetic samples loaded with 1.65% w/w TH (Figure 11e2), which was the faster migration speed for all samples (the migration rate was about 81%). In addition, samples loaded with most TH (2.2%) had a negative influence on cell migration after 72 h (Figure 11f2). The results of wound healing scratch test showed that the core-shell printed matrices were beneficial for cell migration to some extent and samples loaded with 1.65% w/w TH had the maximum effect on promoting cell migration.

3. Conclusion

In conclusion, core-shell printed matrices containing two polymer materials loaded with two drugs were successfully produced in this study. Results suggested that the concentration of PEO solution could influence the coaxial structure of matrices. The resulting core-shell matrices showed accurate stacking and the concentration of TH loaded in PCL component had an effect on coaxial filaments diameter. Besides, adding Fe_3O_4 NPs and varying TH concentration also had the impact on matrices mechanical properties and drug release behaviors. Drug released from the matrices with higher drug

concentration improved the release rate and external AMF also can induced faster release speed for both TH and LH. In-vitro biological evaluation indicated that adding suitable amount of TH (1.1% w/w) could maximum the cell viability and the core-shell printed matrices showed good bioactivity, which have the potential to be applied in wound dressings.

4. Experimental Section

Materials: Polyethylene oxide (PEO) (average molecular weight 9.0×10^5 g/mol) was purchased from Huagao Fine Chemical Co., Ltd., China. Polycaprolactone (PCL, mean Mw = 8×10^4 g/mol) were obtained from Sigma-Aldrich, St Louis, USA. Tetracycline hydrochloride (TH) and lidocaine hydrochloride (LH) were provided by Amersco, USA and Aladdin, China, separately. Fe_3O_4 NPs (mean particle diameter ~ 20 nm) were bought from HWRK Chem, China. Sinopharm Chemical Reagent (China) supplied glacial acetic acid, absolute ethyl alcohol and phosphate buffer saline (PBS, pH = 7.4). Purified water was produced by a Millpore Milli-Q Reference ultra-pure water purifier (USA). All materials were used as received without further purification treatment. All chemicals and reagents used were of analytical grade.

Solution Preparation: PEO solutions were prepared by dissolving known quantities of PEO in glacial acetic acid. The concentrations of PEO in glacial acetic acid were selected as 2, 3, 4, 5 and 6% w/w to find out the optimal PEO concentration for inner layer during coaxial EHD printing process. To achieve complete dissolution, the solutions were mechanically stirred for 8 h (VELP ARE heating magnetic stirrer, Italy) at a constant speed of 300 rpm. After picking out the optimum PEO solution, 5% LH (of the PEO quantity) was added to the PEO mixture. Rhodamine B was added to the PEO solutions (Sigma-Aldrich, USA) to allow detection when used with PCL when observed by optical

microscopy.

PCL solutions were prepared as the shell layer for the core-shell matrices. Five PCL solutions were made and utilized during the printing process. 24 %w/w PCL in acetic acid was used in all solutions. To ensure full dissolution, the mixtures were put on the heating magnetic stirrer (VELP ARE, Italy) and were mechanically stirred for 5 h at a stable speed of ~ 200 rpm. TH was then added to the PCL solutions at concentration of 0.55%, 1.1%, 1.65% and 2.2% w/w of the overall solution, respectively. All the solutions were stirred for a further 2h. The solutions were then magnetized by adding a small amount of Fe_3O_4 NPs (to make concentration of Fe_3O_4 NPs at 0.1% w/w of the PCL quantity). The mixtures were immersed for 2 h in a mild bath sonication to obtain a homogenous suspension. Furthermore, there was another solution without Fe_3O_4 NPs as a control in which the concentrations of PCL and TH were 24% w/w and 1.1% w/w, separately. The PCL solutions were prepared to serve as the shell formulation material, while the PEO solution was used as the inner core material. All the experiments were carried out at the ambient temperature (25℃).

Magnetic core-shell matrix printing: The schematic diagram of the coaxial EHD printing system is shown in Figure 1. The EHD printing platform mainly consisted of three components (Figure 1a): a high-voltage supply generating ~30 kV (Glassman high voltage Inc. series FC, USA), two syringe pumps (KD Scientific KDS100, USA), and a high-resolution X-Y-Z movement stage (Hongxia automatic control equipment Co., Guangzhou, China). PCL solutions and PEO solutions were loaded into two 5 mL syringes which were controlled by two separate syringe pumps. A coaxial printing nozzle (inner needle: ID = 0.2mm and OD = 0.4 mm, outer needle: ID = 1.0 mm and OD = 1.5 mm) was mounted on to the Z-axis and connected to the positive terminal of a high voltage supply. The core access of the nozzle was linked with syringe loaded with PEO solutions while the shell access

of the nozzle was connected to the syringe loaded with PCL solutions via soft silicone tubes as shown in Figure 1b. The conductive glass was placed on the grounded X-Y moving stage as the collection substrate. To launch the EHD printing process, high voltage was applied and the syringe pumps were initiated to simultaneously feed PEO solution and PCL solution to the coaxial nozzle. The deposition of the coaxial PCL/PEO filaments can be flexibly controlled to produce complicated patterns by changing the movement of X-Y-Z stage according to the specific user design. The speed of X-Y-Z stage was within the range 60 mm/s – 100 mm/s. The applied voltage of coaxial EHD printing was fixed within the range 2.6 kV-3.0 kV. The distance between the coaxial nozzle and conductive glass was set at 5.0 mm. To keep the cone-jet stable during the EHD process, flow rates for PCL solution and PEO solutions was set as 0.25 ml/h and 0.1 ml/h, separately. Fabrication proceeded by patterning of the 3D complex PCL/PEO matrices with precise designated fiber layers (10 layers along X-axis, 10 layers along Y-axis, and total 20 layers). All experiments were conducted at the ambient temperature (25 ℃) and relative humidity (40-60%).

Material characterization: The morphology of the resulting wound dressings was investigated using optical microscopy (OM, Phoenix BMX503-ICCF, China) and scanning electron microscopy (SEM, FEI Quanta 650, Netherland). OM was applied to image specific inner structures, which cannot be captured by SEM. For SEM analysis, all samples (structures deposited on microscope glass slides) were mounted on a specimen stub with double-sided conductive tape and coated with a thin layer of platinum for 120s using a sputter coater (1080auto, Cressington Scientific Instruments Ltd., UK) at the current intensity of 25mA to prevent sample charging. SEM images were recorded at an acceleration voltage of 5 kV. In this study, all data exported for analysis was plotted as graphs using Origin software (OriginLab, USA). Fiber diameter were investigated using a statistical distribution

utilizing 50 random fibers for each experimental condition. As for the core/shell ratio measurement for the core-shell matrices, the core/shell ratio of 50 fibers for each experimental condition was counted and a mean value was obtained. Error bars in the graphs represent the mean ± standard deviation.

The hydrophobicity of the wound dressings was investigated via contact angle and interfacial tension analysis (SL2000KB, Kino Industry Co., Ltd, USA). The contact angle of a PBS droplet (1 μL) on the core-shell printed matrices was tested. Fourier Transform Infrared (FTIR) was applied to detect composition, interactions and material stability of the matrices.[53] The KBr pellet pressing method was applied to prepare FTIR samples. In brief, 2 mg of printing samples were immersed in 200 mg of KBr medium by grinding and then compressed into transparent pellets (pressure ~12 MPa). FTIR was then used to scan pellets and the spectrums were obtained by using 20 scans with a resolution of 4 cm^{-1} (4000-500cm^{-1}).

To investigate the effect of addition of Fe_3O_4 NPs and variation of concentrations of TH on mechanical properties of core-shell matrices, tensile tests were studied by a universal materials tester (Zwick/Roell Z020, Zwick, Germany). The selected gauge length was 10 mm, and samples were extended along the fiber axis with a 500 N load cell at the crosshead speed of 10 mm/min at the ambient temperature (25 °C). Core-shell printed samples (1.0 × 3.0 cm) were cut for tensile tests. For each sample set, tests were taken in triplicate after which the mean tensile strength was calculated.

To determine the crystalline structure of each component (PCL, PEO, Fe_3O_4 NPs, LH and TH) in the core-shell printed matrices, the X-ray diffraction (XRD) patterns were analyzed by an X-ray crystal diffractometer (Gemini A Ohra, Oxford, UK). The samples were scanned over a 2-theta range of 5°-60° with a step size of 0.02° at 40 kV and 40 mA.

Drug release from the core-shell matrices: In this study, drug release behaviors of both TH and LH from core-shell matrices were investigated according to a method described in previous study.[50] 30 mg of the core-shell printed matrices were placed in 10 ml of pH 7.4 phosphate buffered saline (PBS) with 200 rpm agitated speed in a HZ-8801K thermostatic oscillator (Taicang Science and Education Factory, China). During drug release period, 3 mL of supernatant was extracted for UV detection (UV-2600 spectrophotometer, Shimadzu, Japan) and replenished with an equal volume of fresh release medium at pre-designed time intervals. Each experiment was conducted in triplicate. The concentration of TH in the supernatant was determined using UV absorption at a wavelength of 364 nm, while the wavelength of LH in UV measurements was 262 nm.

Zero-order, first-order, Higuchi and Korsmeyer-Peppas curve –fitting models were used to investigate the drug release kinetics of TH released from the core-shell printed matrices in the normal release environment (PBS, pH=7.4). Zero-order model can be used to describe the drug dissolution of several types of modified release pharmaceutical systems. In these situations, the drug dissolution from dosage forms that do not disaggregate and release the drug slowly can be represented by the Equation (1):

$$Q_t = Q_0 + K_0 t \tag{1}$$

Where Q_t is the amount of drug released in time t, Q_0 is the initial amount of drug in the solution and K_0 is the release order constant. First order model has also been applied to investigate drug release from those containing water-soluble drugs in porous matrices, and the release of the drug which followed first order Kinetics can be expressed by the Equation (2):

$$\log C = \log C_0 - Kt/2.303 \tag{2}$$

Where C_0 is the initial concentration of drug, K is the first order rate constant, and t is the time.[54] Besides, Higuchi model is usually used to confirm diffusive drug release from a polymer matrix

system, and it can be presented as shown in Equation (3):

$$M_t = k_H t^{\frac{1}{2}} \tag{3}$$

Here, M_t is the quantity of cumulative drug release after time t and k_H is the Higuchi constant. The Korsmeyer-Peppas model is normally used to analyze drug release when the mechanism is not clear. This model is shown as Equation (4):

$$\frac{M_t}{M_\infty} = kt^n \tag{4}$$

Here, M_t is the cumulative quantity of drug released at time t, and M_∞ is the initial drug loading , while k is a constant and n is the release exponent indicating the release mechanism.[50]

Moreover, the impact of an applied magnetic field (AMF) on drug release was studied. An external auxiliary magnetic field (AMF) was generated around a vial containing submerged (in PBS) magnetic core-shell printed matrices. The results from normal release environment without AMF application served as the control group. A sinusoidal alternating electric current was generated via a functional signal generator (AFG1022, Tektronix, USA) and circulated into a copper solenoid after being magnified through a power amplifier (HFVA-42, Foneng Science and Technology Co., Ltd., Nanjing, China). The AMF was delivered with a fixed operating frequency of 40 kHz and the output current was maintained at 0.4 A (induced magnetic strength of 1.5 mT). All experiments were proceeded in triplicate.

Antibacterial activity assay: Antibacterial activity of the core-shell printed matrices against *S. aureus* (ATCC29213, Beijing Century Aoke Biological Tech. Co., Ltd., China) was studied using a modified method.[55] Baird-Parker agar base plates hosting egg-yolk tellurite emulsions were coated with 0.1 ml of suspension containing *S. aureus* (OD = 1.9), using the spread plate method. Following this, the core-shell printed matrices were placed on the agar plates (Φ = 6 cm) which were subsequently

incubated (SHP-080 Biochemical Incubator, Shanghai Jinghong Laboratory Instrument Co., Ltd., Shanghai, China) at 37 °C for 24 h. The area of incubation zone was then measured.

A microplate reader (Multiskan GO, Thermo Fisher Scientific, USA) was also used to detect the antibacterial activity of the core-shell printed matrices against *S. aureus*. The frozen *S. aureus* was restored by incubated in a 7.5% sodium chloride broth in a biochemical incubator at 37 °C for 24 h. 0.1 ml suspension containing *S. aureus* (OD = 1.9) was added into 10 ml 7.5% sodium chloride broth. 90 mg of five variations of core-shell printed matrices were added to the five treatment groups, separately. All the samples were incubated at 37 °C for 24 h. The absorbance values of these samples were detected at a wavelength of 371 nm using the microplate reader. As the control samples did not contain the matrices, the anti-bacterial activity could not be observed. The value of control group was set at 100% and the treatment groups values were measured by dividing the value of control group.

Cell culture: For the aim of applying core-shell printed matrices as wound dressings, the matrices should have low toxicity and good biocompatibility. The biocompatibility of core-shell printed matrices was determined using in vitro cell culture assessment. L929 mouse fibroblast cell lines (obtained from American Type Culture Collection, ATCC) were cultured in Modified eagle's medium with 1% antibiotic and antimycotic MEM medium (Genom Biomedical Technology Co., LTD, China). 10% fetal bovine serum (FBS, Gibco, USA) was also added into the 9 cm diameter cell culture dishes at 37 °C at humidified atmosphere (5% CO_2). The culture medium needed to be changed every 48 h. All the samples applied in cell tests were sterilized under UV light for 24 h and then fixed with sterilized stainless-steel rings in the culture dish. L929 cells were seeded on five different kinds of core-shell printed matrices (density of 1.0×10^5 cells/cm^2).

Investigation of cell morphology: After 3 days culture, cell morphology was investigated according

to a previously reported method.[30] L929 cells cultured on matrices were fixed using 4% (v/v) formalin for 20 min at the ambient temperature (25°C), and were washed 3 times by PBS (pH = 7.4). Cells were then permeabilized with 0.1% Triton X-100 in PBS for 5 min. After washed by PBS, cell cytoskeleton and nuclei were stained with Alexar Fluor 546 phalloidine (Yeasen Biology Technology Co., LTD, China) (1:100 dilution) and 4',6'-diamidino-2-phenylindole hydrochloride (DAPI, Yeasen Biology Technology Co., LTD, China) for 20 and 5 min, separately. Then the samples were washed 3 times (PBS) after each staining step. After that, cells were observed by an inverted fluorescent microscope (Nikon, Eclipse Ti-S, Japan).

Cell viability test: An amount of 100 μL L929 cell suspension was transferred to a 96-well plate at a density of 1×10^4 cells/well and was incubated for 24 h. CCK-8 test was conducted to evaluate proliferation of L929 cells on five different kinds of core-shell printed matrices after 3 days during cell culture. The matrices were cut into discs (diameter = 6 mm) and sterilized under UV light for 24 h and then added to the cell culture plate. After incubation for 3 days, cell viability was measured by adding 10 μL of CCK-8 solution to each well and incubated for a further 4 h. Absorbance was detected at a wavelength of 450 nm by a microplate reader (Multiskan GO, Thermo Fisher Scientific, USA). Cell viability in TCPs well plate (only) was used as control and the culture medium with CCK-8 solution was served as a blank. The relative cell viability (%) was calculated using Equation (5):

$$\text{Cell viability (\%)} = \frac{Ab.(sample) - Ab.(blank)}{Ab.(control) - Ab.(blank)} \times 100\% \qquad (5)$$

Where Ab. means the absorbance.

In vitro scratch assay: The migration behavior of L929 cells treated with different samples was assessed through the wound healing assay.[56] The matrices samples were sterilized by UV-light for

24 h. L929 cells were seeded in a 6 well TCPs plate with a density of 3×10^5 cells/well and incubated

at 37 °C in 5% CO_2 in a humidified atmosphere till confluent and formation of monolayers. Using a

200 µL sterile pipette tip, a scratch was made on the monolayer cell surface and gently washed with

PBS to remove the free cells from the scratched area. The refresh medium is added to the scratched

well and incubated at 37 °C and 5% CO_2 in a humidified atmosphere. Images of the scratches were

captured at 0, 24, and 72h using an inverted fluorescent microscope (Nikon, Eclipse Ti-S, Japan) to

observe the cell migration in the scratched area.

References

[1]   D. Liang, Z. Lu, H. Yang, J. Gao, R. Chen, *Acs. Appl. Mater. Inter.* **2016**, *8*, 3958.

[2]   M. Liu, G. Luo, Y. Wang, R. Xu, Y. Wang, W. He, J. Tan, M. Xing, J. Wu, *Sci. Rep.* **2017**, *7*, 436.

[3]   S. Napavichayanun, P. Amornsudthiwat, P. Pienpinijtham, P. Aramwit, *Mater. Sci. Eng. C-Mater. Biol. Appl.* **2015**, *55*, 95.

[4]   A. Chiarini, G. Freddi, D. Liu, U. Armato, I. Dal Prà, *Tissue.Eng. Part. A.* **2016**, *22*, 1047.

[5]   R. Lalani, L. Y. Liu, *Biomacromolecules.* **2012**, *13*, 1853.

[6]   R. Xu, G. Luo, H. Xia, W. He, J. Zhao, B. Liu, J. Tan, J. Zhou, D. Liu, Y. Wang, *Biomaterials.* **2015**, *40*, 1.

[7]   A. GhavamiNejad, A. Rajan Unnithan, A. Ramachandra Kurup Sasikala, M. Samarikhalaj, R. G. Thomas, Y. Y. Jeong, S. Nasseri, P. Murugesan, D. Wu, C. Hee Park, *Acs. Appl. Mater. Inter.* **2015**, *7*, 12176.

[8]   C. Wu, G. Zhang, T. Xia, Z. Li, K. Zhao, Z. Deng, D. Guo, B. Peng, *Mater. Sci. Eng. C-Mater. Biol. Appl.* **2015**, *55*, 155.

[9]   A. W. C. Chua, Y. C. Khoo, B. K. Tan, K. C. Tan, C. L. Foo, S. J. Chong, *Burns. Trauma.* **2016**, *4*, 14.

[10]   G. D. Liu, Z. B. Gu, Y. Hong, L. Cheng, C. M. Li, *J. Control. Release.* **2017**, *252*, 95.

[11]   R. Shi, H. Geng, M. Gong, J. J. Ye, C. G. Wu, X. H. Hu, L. Q. Zhang, *J. Colloid. Interf. Sci.* **2018**, *509*, 275.

[12]   K. S. Rho, L. Jeong, G. Lee, B. M. Seo, Y. J. Park, S. D. Hong, S. Roh, J. J. Cho, W. H. Park, B. M. Min, *Biomaterials.* **2006**, *27*, 1452.

[13]   S. A. Castleberry, B. D. Almquist, W. Li, T. Reis, J. Chow, S. Mayner, P. T. Hammond, *Adv.Mater.* **2016**, *28*, 1809.

[14]   R. Feng, R. Fu, Z. Duan, C. Zhu, X. Ma, D. Fan, X. Li, *J. Biomat. Sci-Polym. E.* **2018**, *29*, 1463.

[15]   Q. Huang, Y. Zhu, *Adv. Mater. Technol.* **2019**, *4*, 1800546.

[16]   Y. Han, J. Dong, *Adv. Mater. Technol.* **2018**, *3*, 1700268.

[17]   S. Wu, J. Li, J. Mai, M. Chang, *ACS applied materials & interfaces* **2018**, *10*, 24876.

[18]   A. P. M. Madrid, S. M. Vrech, M. A. Sanchez, A. P. Rodriguez, *Mat. Sci. Eng. C-Mater.* **2019**, *100*, 631.

[19]   R. Thakur, C. Florek, J. Kohn, B. Michniak, *Int. J. Pharmaceut.* **2008**, *364*, 87.

[20]   V. M. Merkle, P. L. Tran, M. Hutchinson, K. R. Ammann, K. DeCook, X. Y. Wu, M. J. Slepian, *Acta. Biomater.* **2015**, *27*, 77.

[21]   A. A. El-Shanshory, W. M. Chen, H. A. El-Hamshary, S. S. Al-Deyab, X. M. Mo, *J. Control. Release.* **2015**, *213*, E8.

[22]   P. Zahedi, I. Rezaeian, S.-O. Ranaei-Siadat, S.-H. Jafari, P. Supaphol, *Polym. Advan. Technol.* **2010**, *21*, 77.

[23]   B. Wang, H. Zheng, M. Chang, Z. Ahmad, J. Li, *Colloid. Surf. B.* **2016**, *145*, 757.

[24]   A. Cipitria, A. Skelton, T. Dargaville, P. Dalton, D. Hutmacher, *J. Mater. Chem.* **2011**, *21*, 9419.

[25]   X. Hu, Y. Wang, L. Zhang, M. Xu, J. Zhang, W. Dong, *Int. J. Biol. Macromol.* **2018**, *108*, 558.

[26]   T.-Y. Liu, S.-H. Hu, T.-Y. Liu, D.-M. Liu, S.-Y. Chen, *Langmuir.* **2006**, *22*, 5974.

[27]   J. An, H. Zhang, J. Zhang, Y. Zhao, X. Yuan, *Colloid. Polym. Sci.* **2009**, *287*, 1425.

[28]   A. Popescu, R. S. Salcido, *Adv. Skin. Wound. Care.* **2004**, *17*, 14.

[29]   O. N. Aydin, M. Eyigor, N. Aydin, *Eur. J. Anaesth.* **2001**, *18*, 687.

[30]   B. Wang, S. Wu, Z. Ahmad, J.-S. Li, M.-W. Chang, *Eur. Polym. J.* **2018**, *104*, 81.

[31]   A. Lee, H. Jin, H.-W. Dang, K.-H. Choi, K. H. Ahn, *Langmuir.* **2013**, *29*, 13630.

[32]   B. Wang, Z. Ahmad, J. Huang, J.-S. Li, M.-W. Chang, *Chem. Eng. J.* **2018**, *343*, 379.

[33]   J. C. Wang, H. Zheng, M. W. Chang, Z. Ahmad, J. S. Li, *Sci. Rep.* **2017**, *7*, 43924.

[34]   J. C. Wang, M. W. Chang, Z. Ahmad, J. S. Li, *J. Drug Deliv. Sci.* **2016**, *35*, 114.

[35]   P. Singh, S. J. Desai, A. P. Simonelli, W. I. Higuchi, *J. Pharm. Sci.* **2010**, *57*, 217.

[36]   Y. Z. Zhang, H. W. Ouyang, C. T. Lim, S. Ramakrishna, Z. M. Huang, *J. Biomed. Mater. Res. B.* **2005**, *72B*, 156.

[37]   T. Briggs, T. L. Arinzeh, *J. Biomed. Mater. Res. A.* **2014**, *102*, 674.

[38]   D. W. Ding, X. R. Yan, X. Zhang, Q. L. He, B. Qiu, D. W. Jiang, H. G. Wei, J. Guo, A. Umar, L. Y. Sun, Q. Wang, M. A. Khan, D. P. Young, X. Zhang, B. Weeks, T. C. Ho, Z. H. Guo, S. Y. Wei, *Superlattice. Microst.* **2015**, *85*, 305.

[39]   S. Ramesh, T. F. Yuen, C. J. Shen, *Spectrochim. Acta. A.* **2008**, *69*, 670.

[40]   F. Shahrzad, A. M. Ali, G. Azadeh, K. Mojtaba, *J. Biomed. Mater. Res. A.* **2015**, *103*, 3852.

[41]   Y. Huangfu, C. Liang, Y. Han, H. Qiu, P. Song, L. Wang, J. Kong, J. Gu, *Composites Science and Technology* **2019**, *169*, 70.

[42]   C.-W. Chou, S.-h. Hsu, H. Chang, S.-M. Tseng, H.-R. Lin, *Polym. Degrad. Stab.* **2006**, *91*, 1017.

[43]   F. A. Sheikh, N. A. Barakat, M. A. Kanjwal, A. A. Chaudhari, I.-H. Jung, J. H. Lee, H. Y. Kim, *Macromol. Res.* **2009**, *17*, 688.

[44] M. Sattary, M. T. Khorasani, M. Rafienia, H. S. Rozve, *Polym. Advan. Technol.* **2018**, *29*, 451.

[45] P. Mehdi, H. Marie-Claude, A. Abdellah, *Biomacromolecules.* **2012**, *13*, 412.

[46] K. Nazari, E. Kontogiannidou, R. H. Ahmad, A. Gratsani, M. Rasekh, M. S. Arshad, B. S. Sunar, D. Armitage, N. Bouropoulos, M.-W. Chang, X. Li, D. G. Fatouros, Z. Ahmad, *Eur. J. Pharm. Sci.* **2017**, *102*, 147.

[47] N. J. Babu, A. Nangia, *Cryst. Growth. Des.* **2011**, *11*, 2662.

[48] X. D. Wang, Y. J. Wang, K. Wei, N. R. Zhao, S. H. Zhang, J. D. Chen, *J. Mater. Process. Technol.* **2009**, *209*, 348.

[49] K. Kim, Y. K. Luu, C. Chang, D. F. Fang, B. S. Hsiao, B. Chu, M. Hadjiargyrou, *J. Control. Release.* **2004**, *98*, 47.

[50] Y. Gao, M. W. Chang, Z. Ahmad, J. S. Li, *Rsc. Adv.* **2016**, *6*, 88157.

[51] Y. Kang, C. Wang, Y. Qiao, J. Gu, H. Zhang, T. Peijs, J. Kong, G. Zhang, X. Shi, *Biomacromolecules* **2019**, *20*, 1765.

[52] Z. C. Yao, S. C. Chen, Z. Ahmad, J. Huang, M. W. Chang, J. S. Li, *J. Food. Sci.* **2017**, *82*, 1412.

[53] Y. Guo, Z. Lyu, X. Yang, Y. Lu, K. Ruan, Y. Wu, J. Kong, J. Gu, *Composites Part B-Engineering* **2019**, *164*, 732.

[54] S. Dash, P. N. Murthy, L. Nath, P. Chowdhury, *Acta. Pol. Pharm.* **2010**, *67*, 217.

[55] L. F. Zhu, J. S. Li, J. Mai, M. W. Chang, *Chem. Eng. J.* **2019**, *357*, 498.

[56] G. Perumal, S. Pappuru, D. Chakraborty, A. M. Nandkumar, D. K. Chand, M. Doble, *Mat. Sci. Eng. C-Mater.* **2017**, *76*, 1196.

Figures and Tables
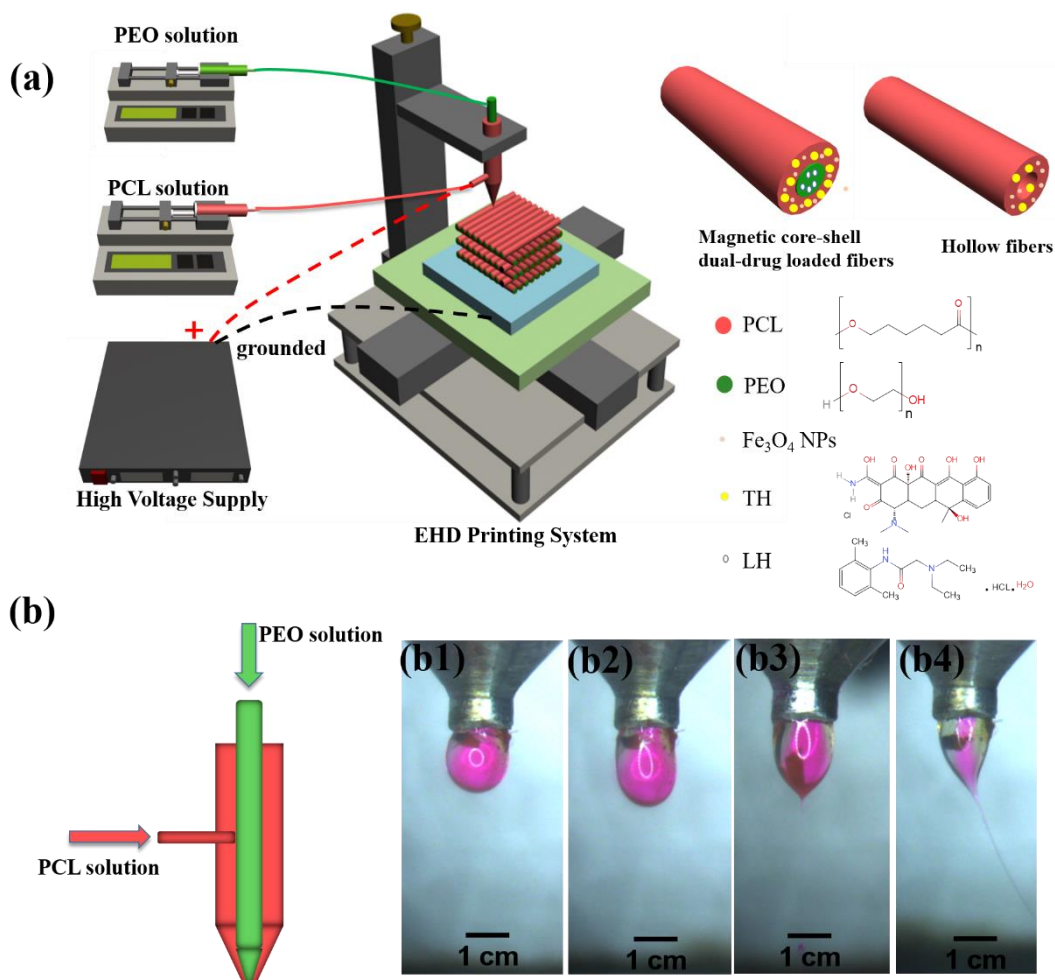
Figure 1. (a) Schematic diagram of the coaxial EHD printing system. (b) Details of the coaxial EHD printing nozzle. (b1) - (b4) Experimental images of the coaxial jet during the process increasing the applied voltage of EHD printing. The applied voltages of (b1-b4) are 0 kV, 1.5 kV, 2.0 kV and 2.6 kV, separately.
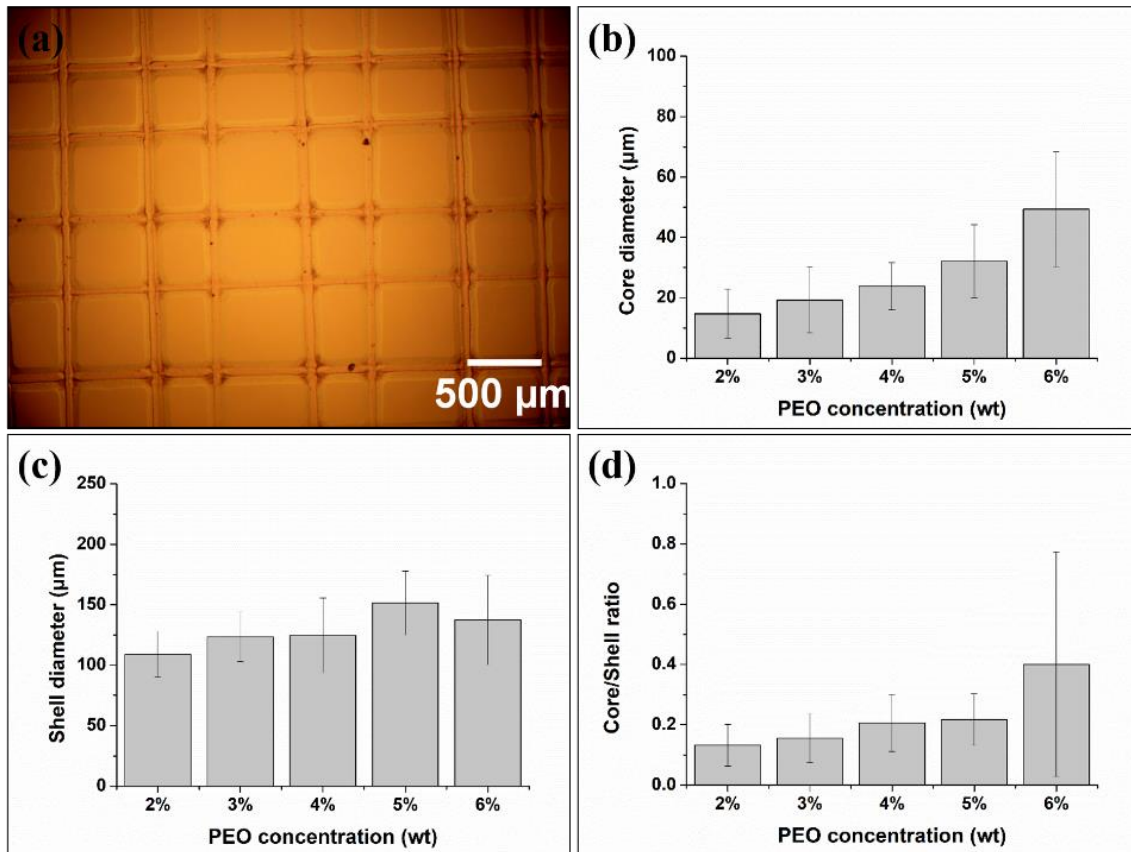
Figure 2. (a) Optical micrograph of coaxial EHD printing structures when the concentration of PEO was set at 5% w/w. (b) Core diameter (c) Shell diameter (whole fiber diameter) and (d) Core/shell ratio varies with increasing PEO concentrations. All the images were obtained when the speed of X-Y-Z stage was at 80mm/s.
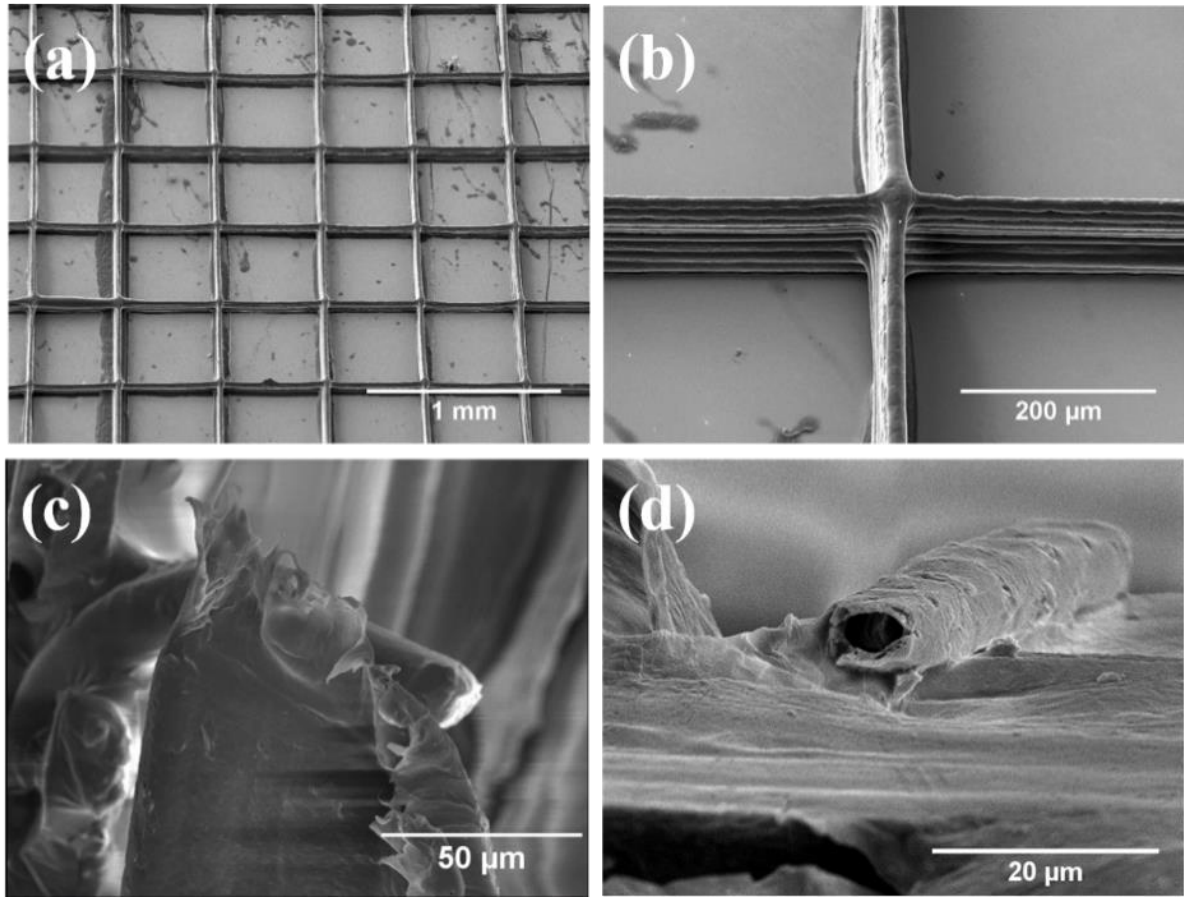
Figure 3. (a)-(b) The SEM images with different magnifications of core-shell printed matrices loaded without Fe$_3$O$_4$ NPs and with 1.1% TH in PCL layer. The SEM image of cross-section of this kind of core-shell fibers (c) before and (d) after the matrices immersed in DI water. All images were obtained under the situation that inner flow rate and outer flow rate were 0.1 ml/h and 0.25ml/h, respectively; the applied voltage was 2.6 kV and the move speed of X-Y-Z stage was 80 mm/s.
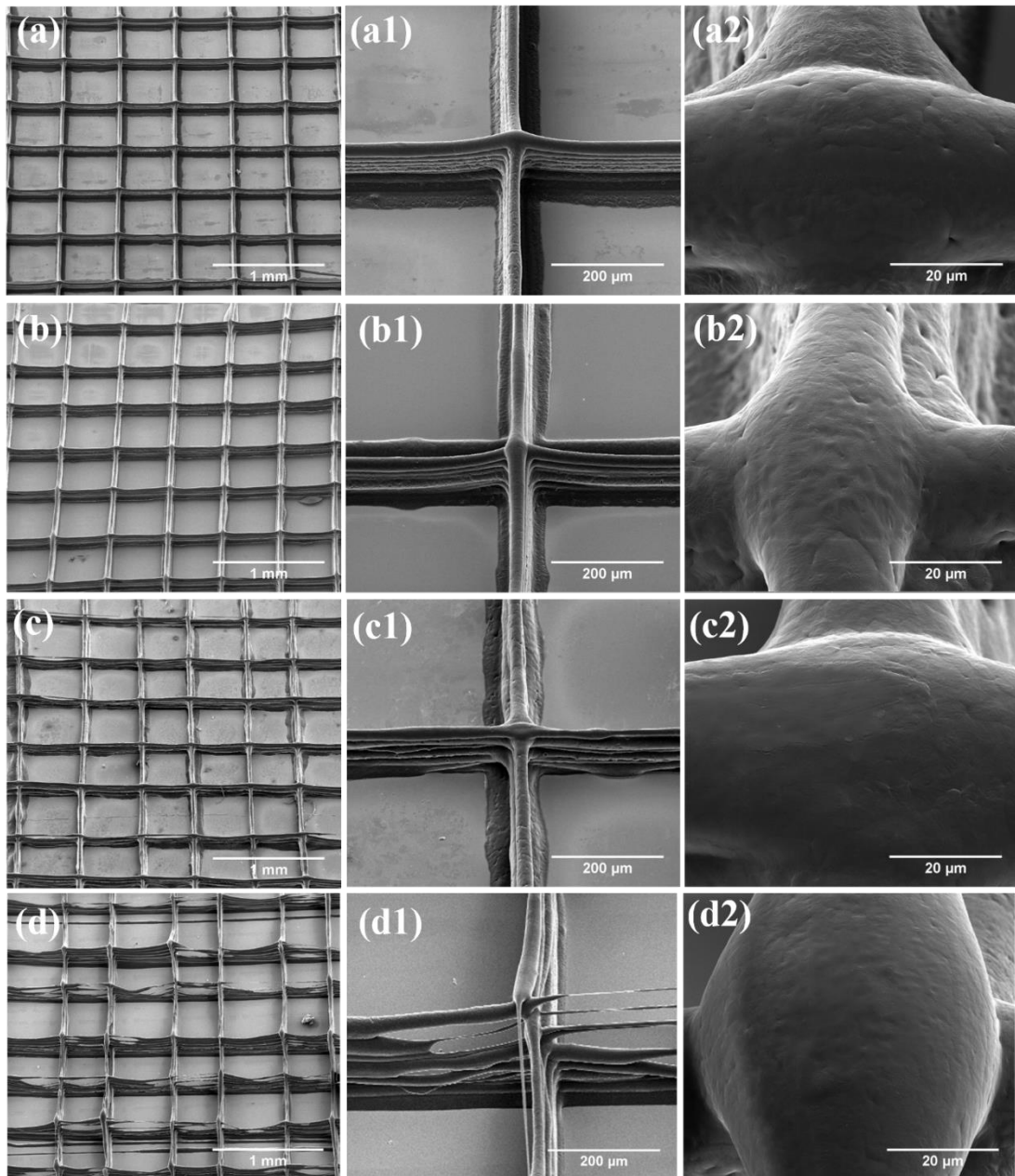
Figure 4. Inclined SEM images of magnetic core-shell printed coaxial EHD printing matrices (a) 0.55% w/w TH; (b) 1.1% w/w TH; (c) 1.65% w/w TH and (d) 2.2% w/w TH. (a1) -(d2) are SEM images with higher magnification. All images were obtained under the situation that inner flow rate and outer flow rate were 0.1 mL/h and 0.25 mL/h, respectively; the applied voltage was 2.6 kV and the move speed of X-Y-Z stage was 80 mm/s.
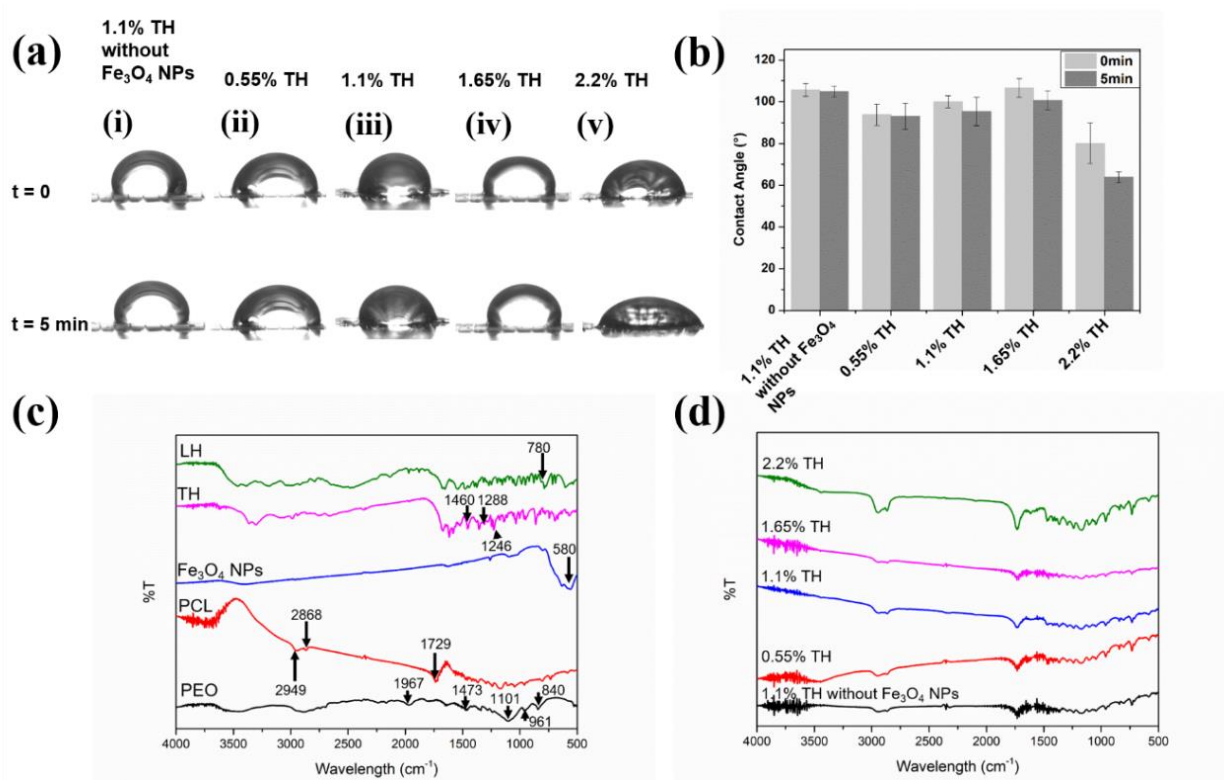
Figure 5. (a) Real time optical images of contact angles of five different kinds of matrices at t = 0 min and t = 5 min. (b) Detailed values of contact angles which are accordance with (a). (c) FTIR spectrum of pure PCL, PEO, Fe_3O_4 NPs, TH and LH. (d) FTIR spectrum of five kinds of matrices.
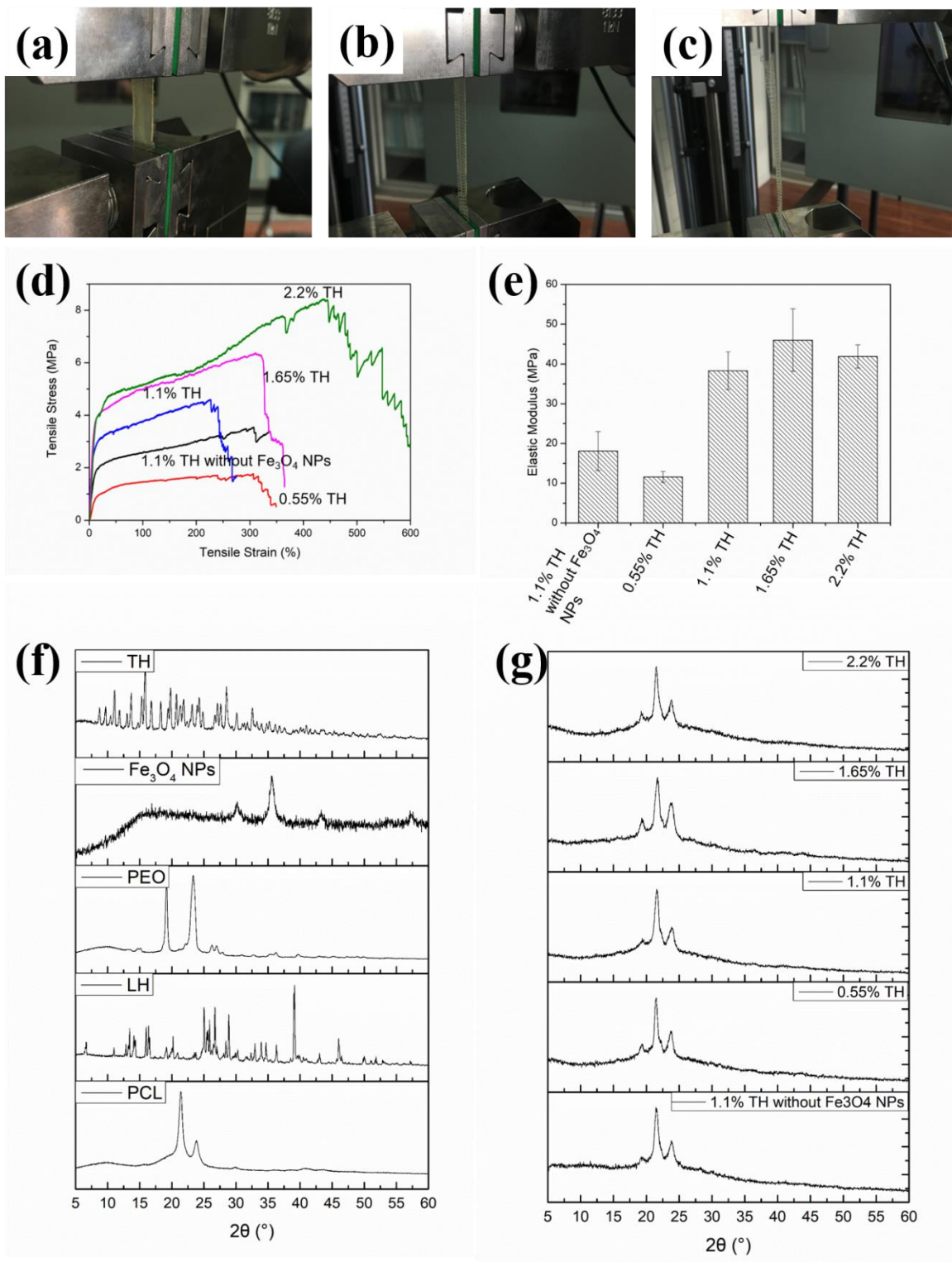
Figure 6. The (a) start (b) process (c) end of mechanical test for core-shell printed matrices loaded with Fe$_3$O$_4$ NPs and 1.1% w/w TH. (d) Stress-strain curves and (e) elastic modulus for five kinds of core-shell printed matrices. (f) XRD patterns of pure TH, Fe$_3$O$_4$ NPs, PEO, LH and PCL. (g) XRD patterns of five kinds of core-shell printed matrices.
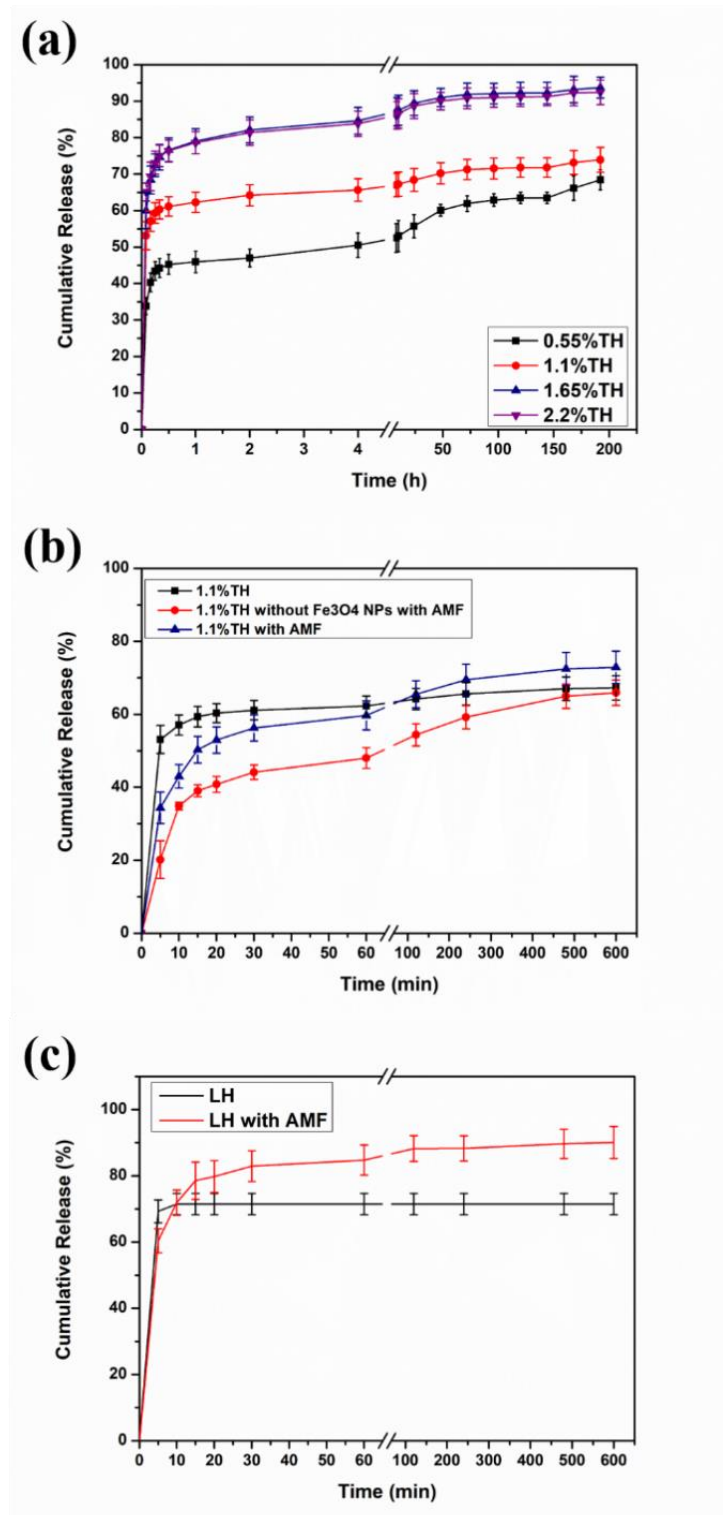
Figure 7. (a) TH release profiles from core-shell printed matrices loaded with 0.55%, 1.1%, 1.65%, and 2.2% w/w TH. (b) TH release curves for magnetic and non-magnetic matrices loaded with 1.1% w/w TH with the aid of an external AMF. (c) The release profiles of LH from core-shell printed matrices with and without AMF.
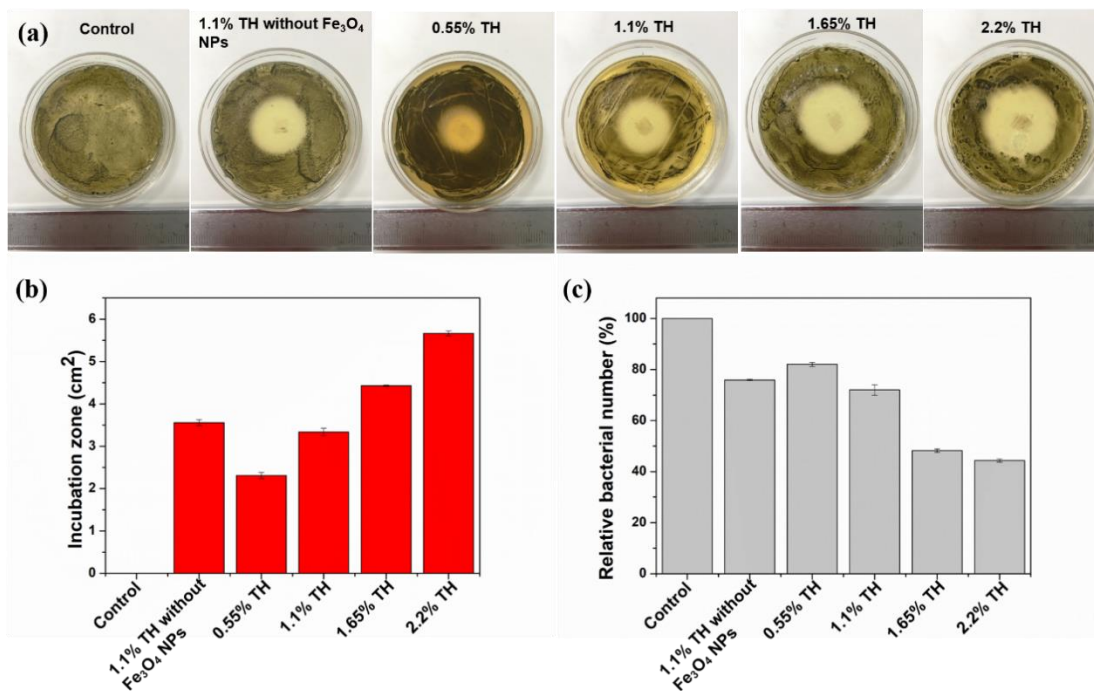
Figure 8. (a) Inhibition zones for disc samples of matrices against *S. aureus* after 24 h incubation. (b) Inhibition zone area of control group and five different kinds of matrices groups. (c) Antibacterial activity against *S. aureus* using a microplate reader.
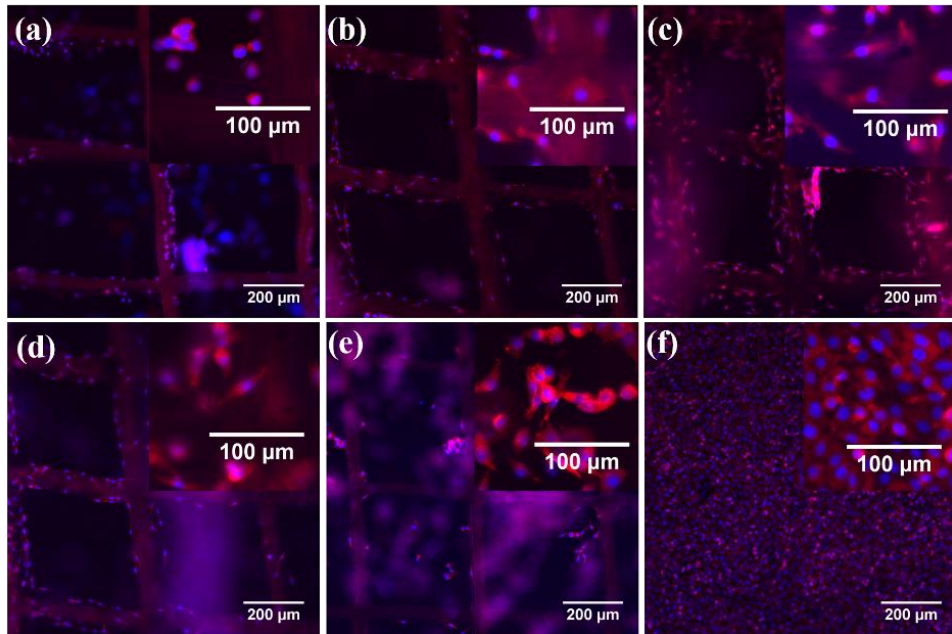
Figure 9. Fluorescent images of cell cultured on core-shell printed matrices loaded with (a) 1.1% w/w TH and without Fe_3O_4 NPs (b) 0.55% w/w TH (c) 1.1% w/w TH (d) 1.65% w/w TH (e) 2.2% w/w TH and (f) control (culture dish without samples).
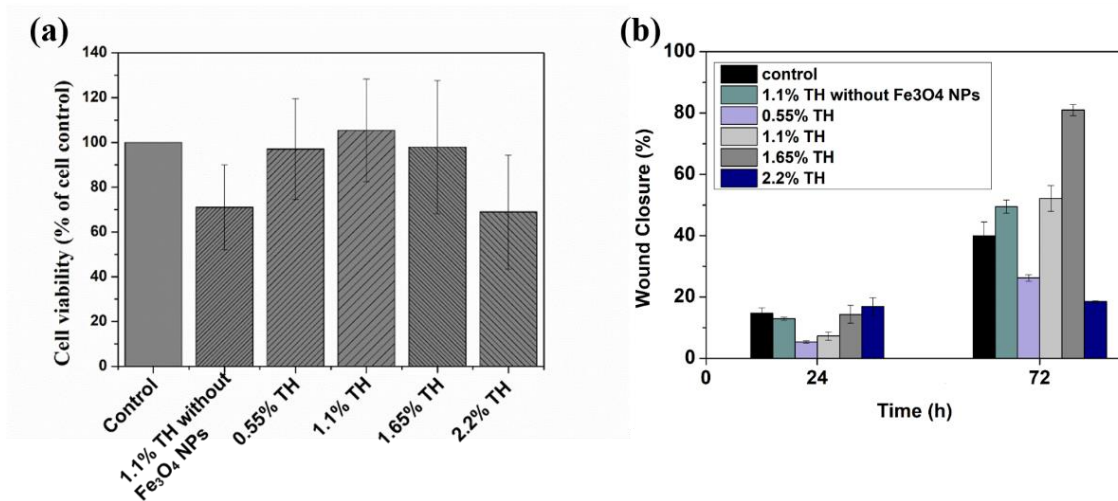

Figure 10. (a) CCK-8 test on five kinds of core-shell printed matrices after 3 days culture. And the control was the cells cultured just on the 96-well plate. (b) Quantification of the scratch by the curves of the percentage of gap closure as a function of incubation time.
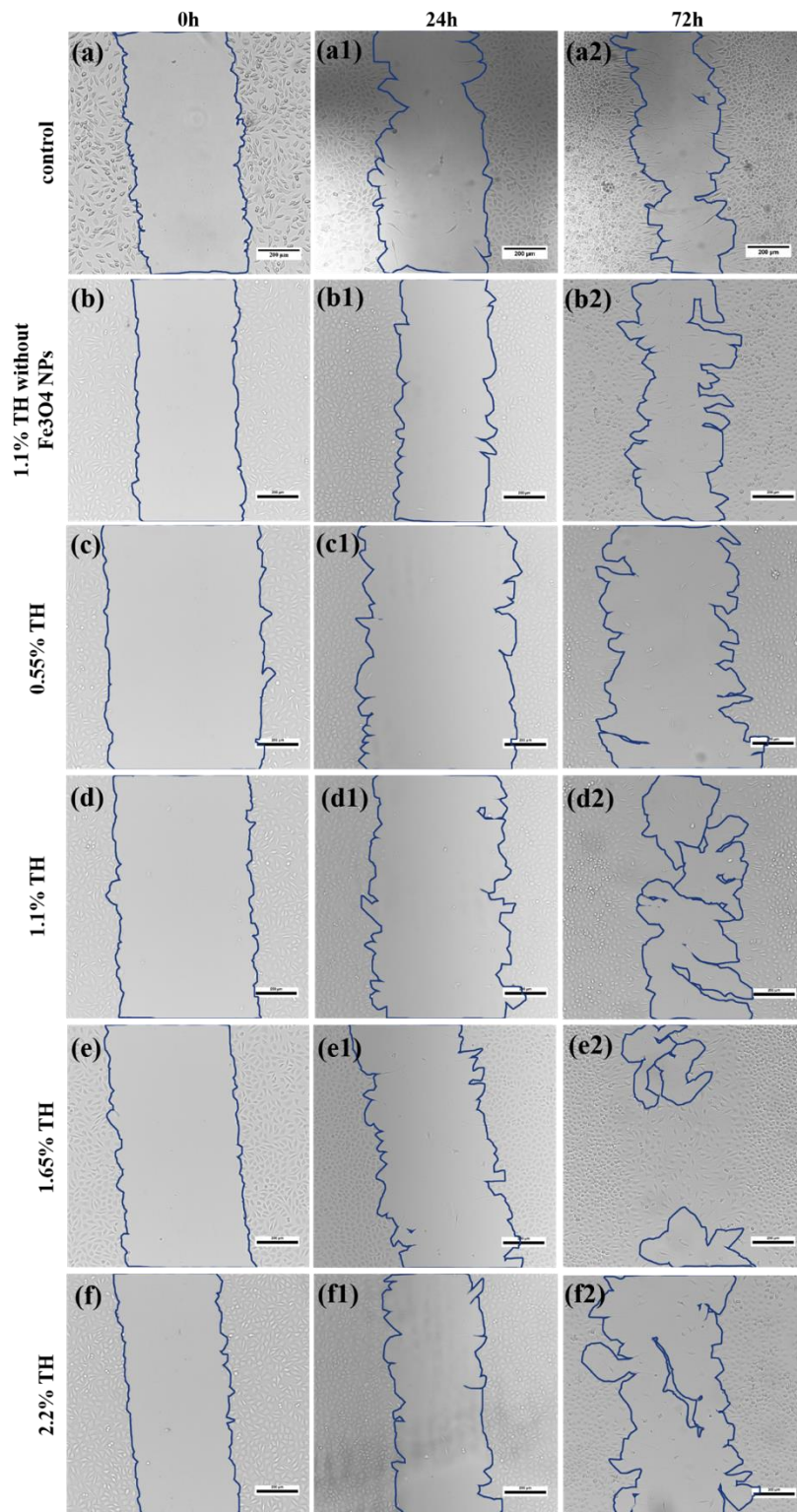
Figure 11. Illustrative micrographs of L929 cells migrating into a scratch area over a 72 h period in (a) the absence (control), (b) the non-magnetic samples and magnetic samples loaded with (c) 0.55%, (d) 1.1%, (e) 1.65% and (f) 2.2% w/w TH. The blue lines in these images showed the edges of scratch area.

Table 1. Fitting Parameters of TH release from core-shell printed matrices loaded with 0.55%, 1.1%, 1.65%, and 2.2% w/w TH.

Release samples	Zero-order (R^2)	First-order (R^2)	Higuchi (R^2)	Korsmeyer-Peppas (R^2)	n
0.55% w/w TH	0.7261	0.6440	0.8763	0.96045	0.0719
1.1% w/w TH	0.5958	0.5557	0.7693	0.9568	0.0346
1.65% w/w TH	0.4398	0.3935	0.6258	0.8786	0.0444
2.2% w/w TH	0.4835	0.4483	0.6772	0.9306	0.0389